Identification of a Contact Domain between Echistatin and the Integrin $\alpha_v\beta_3$ by Photoaffinity Cross-Linking†

Lukas Scheibler,‡ Dale F. Mierke,§ Gal Bitan,‡,# Michael Rosenblatt,‡ and Michael Chorev*,‡

Division of Bone and Mineral Metabolism, Charles A. Dana and Thorndike Laboratories, Department of Medicine, Beth Israel Deaconess Medical Center and Harvard Medical School, 330 Brookline Avenue, Boston, Massachusetts 02215, and Departments of Chemistry and Molecular Pharmacology, Division of Biology and Medicine, Brown University, Providence, Rhode Island 02912

Received May 4, 2001; Revised Manuscript Received October 1, 2001

ABSTRACT: The integrin $\alpha_v\beta_3$ is the major receptor mediating the attachment of osteoclasts to the extracellular matrix in bone and plays a critical role in bone resorption and bone remodeling. Most of the ligands interacting with the $\alpha_v\beta_3$ receptor contain an Arg-Gly-Asp (RGD) motif. Recently, we have identified two small RGD peptides, containing a benzophenone moiety at either the carboxyl or amino terminus, that photo-cross-linked within the β_3[99−118] [Bitan, G., et al. (1999) *Biochemistry 38*, 3414−3420] or the β_3[167−171] [Bitan, G., et al. (2000) *Biochemistry 39*, 11014−11023] sequence, respectively, of the $\alpha_v\beta_3$ receptor in a selective fashion. Here, we report the synthesis of a photoreactive analogue of echistatin (a 49-amino acid peptide), a potent RGD-containing antagonist of the $\alpha_v\beta_3$ receptor both in vitro and in vivo. This bioactive analogue is substituted at position 45 with a *p*-benzoyl moiety (*p*Bz$_2$), located within the flexible C-terminal domain and removed 20 amino acid residues from the $R^{24}GD^{26}$ triad. This C-terminal domain was reported to contribute to receptor binding affinity by acting as an auxiliary binding site. The radiolabeled ^{125}I-[Arg^{35},Lys^{45}(N^{ϵ}-*p*Bz$_2$)]-echistatin photo-cross-links effectively to a site within the β_3[209−220] sequence. Residues in this domain have been reported to be part of the metal ion-dependent adhesion site (MIDAS). Receptor fragments overlapping this domain were reported to bind to fibrinogen and block fibrinogen binding to $\alpha_{IIb}\beta_3$, the platelet integrin receptor. Taken together, position 45 in echistatin, located within an auxiliary binding site in echistatin, cross-links to a site distinct from the two previously reported sites, β_3[99−118] and β_3[167−171], which cross-link to photophores flanking the RGD triad. These cross-linking data support the hypothesis that the ligand-bound conformation of the integrin β_3 subunit differs from the known conformation of I domains.

Integrins are heterodimeric cell surface adhesion molecules which play pivotal roles in diverse cellular processes such as cell migration, proliferation, and attachment (*1*). The $\alpha_v\beta_3$ integrin (vitronectin receptor) is the most abundant integrin receptor expressed by human osteoclasts, the multinucleated cells responsible for bone resorption. This receptor is thought to participate not only in the attachment of the cell to the bone matrix (*2*, *3*) but also in transcytosis of the dissolved bone matrix components from the resorption lacuna across the cell to the extracellular fluid compartment (*4*−*6*). Antagonists of the $\alpha_v\beta_3$ receptor block bone resorption both in vitro and in vivo (*3*, *7*−*10*), thus providing a novel mechanism-based potential approach to the prevention and treatment of bone diseases such as osteoporosis. Osteoporosis results from excessive bone resorption, which leads to loss of bone mass, compromised bone mechanical strength, and eventually to high frequency of bone fractures.

The integrins are composed of two subunits, each containing a large N-terminal extracellular domain, a transmembrane domain, and a small C-terminal intracellular portion. Due to the large size of the $\alpha_v\beta_3$ receptor and its membranal localization, it is not amenable to analysis by X-ray and nuclear magnetic resonance techniques, and therefore, high-resolution structural data of this complex are not available. Structural studies depend therefore on low-resolution techniques such as electron microscopy (*11*, *12*), receptor mutagenesis studies (*13*, *14*), generation of integrin-activating or inhibitory antibodies (*15*−*20*), and various forms of affinity labeling (*21*−*27*). Importantly, most of the structural information on integrin receptors now available was acquired for receptors other than $\alpha_v\beta_3$ and, therefore, may not be of immediate applicability for understanding the specific ligand−receptor interactions of this receptor system.

Photoaffinity cross-linking covalently locks the specific bimolecular interaction between the photophore-carrying amino acid residue, in the ligand, and the contact site, in the receptor, by generating a bond between the ligand and the receptor. Subsequently, specific chemical or enzymatic cleavages generate particular ligand−receptor-conjugated

† This work was supported in part by Grant AR42833 (to M.R.) from the National Institute of Arthritis and Musculoskeletal and Skin Diseases of the National Institutes of Health and by a postdoctoral fellowship (to L.S.) from the Swiss National Science Foundation.

* To whom correspondence should be addressed: Division of Bone and Mineral Metabolism, Beth Israel Deaconess Medical Center, 330 Brookline Ave. (HIM 944), Boston, MA 02215. Telephone: (617) 667-0901. Fax: (617) 667-4432. E-mail: michael_chorev@hms.harvard.edu.

‡ Beth Israel Deaconess Medical Center and Harvard Medical School.

§ Brown University.

Current address: Center for Neurologic Diseases, Brigham and Women's Hospital and Harvard Medical School, 77 Ave. Louis Pasteur (HIM 750), Boston, MA 02115.

10.1021/bi0109156 CCC: $20.00
Published on Web 11/22/2001

fragments that contain the photoinsertion site. Assignment of the size of the fragments by PAGE[1] analysis is used in the subsequent analysis of the putative digestion maps to identify the contact site. This methodology manifests the only direct approach to studying ligand−receptor bimolecular interactions. Reiteration of this process with ligands modified singularly at discrete positions by the photophore comprises the photoaffinity scanning (PAS) approach (*28*) which complements nicely the receptor mutagenesis and ligand structure−activity studies. The two latter approaches are receptor- and ligand-based, respectively, and therefore are mutually "blind" to the interacting counterpart. Currently, PAS is the method of choice for directly mapping the bimolecular ligand−receptor interface in an effort to generate an experimentally based model of ligand−receptor complexes. Such studies were recently reported for the parathyroid hormone (*29*), vasopressin (*30*), secretin (*31*, *32*), and cholecystokinin receptors (*33*).

Recently, using the PAS approach, we identified two small arginyl-glycyl-aspartyl (RGD)-containing peptides, substituted with a benzophenone (BP) photophore at either the carboxyl or the amino terminus, which photo-cross-linked within the β_3[99−118] (*21*) or β_3[167−171] (*27*) sequence, respectively, of the $\alpha_v\beta_3$ receptor in a selective fashion, thus identifying two contact sites that belong to the ligand−receptor bimolecular interface. In combination with molecular models generated by homology modeling, these results challenge the prevailing structural model of the ligand-binding site of the β_3 subunit. In particular, a direct interaction between the ligand and the metal-ion dependent adhesion site (MIDAS) in β_3 appears to be unlikely or would require a globular fold different from the published one (*34*).

The endogenous ligands for the $\alpha_v\beta_3$ receptor are proteins containing an RGD motif, including vitronectin, bone sialoprotein, and osteopontin. However, many of these protein−ligand complexes are not specific for the vitronectin receptor, but are also recognized by other integrin receptor subtypes. High-affinity and often subtype-selective RGD-containing proteins, namely, disintegrins, have been found in snake venoms. One of these is echistatin, originally isolated from the viper *Echis carinatus* (*35*), which is a potent inhibitor of the $\alpha_v\beta_3$ and $\alpha_{IIb}\beta_3$ integrins. It contains 49 amino acids and four disulfide bridges.

NMR studies of echistatin reveal a rigid globular fold, stabilized by the four disulfide bridges, a flexible RGD-containing loop, and a flexible C-terminal domain (*36*, *37*). The RGD triad, located at the top of the hairpin in the mobile loop has been shown to be important for irreversible binding to the $\alpha_v\beta_3$ receptor (*38*, *39*). The flexible C-terminal domain of echistatin is thought to contribute to receptor binding affinity by acting as an auxiliary binding site, interacting with an exosite on the receptor. Indeed, a linear peptide representing this region, echistatin(40−49), was able to inhibit binding of $\alpha_{IIb}\beta_3$ to immobilized echistatin (*40*). Interestingly, the P^{40}-R-N-P^{43} motif at the C-terminal region of echistatin is homologous with the P^{286}-R-N-P^{289} and P^{829}-R-N^{831} motifs in human fibrinogen α_E. The latter sequence is within the α_EC domain of fibrinogen that interacts specifically with the $\alpha_v\beta_3$ receptor (*41*).

The current photo-cross-linking study was carried out in an effort to better understand the role of the C-terminal region of echistatin in binding to human $\alpha_v\beta_3$ and to further characterize the interface of the $\alpha_v\beta_3$−ligand ternary complex. We designed and synthesized ^{125}I-[Arg^{35},Lys^{45}(N^{ϵ}-*p*Bz_2)]-echistatin [^{125}I-K^{45}(BP)], a potent radioiodinated echistatin analogue containing a photoreactive moiety at position 45 located at the C-terminal region. Characterization of the echistatin−$\alpha_v\beta_3$ receptor photoconjugate and analysis of its chemical and enzymatic cleavage products reveal a short domain, 12 amino acids in length, corresponding to the β_3[209−220] sequence which includes a site of contact with position 45 in the C-terminus of echistatin. Modeling based on our cross-linking data of the C-terminal region of echistatin with the β_3 subunit in the $\alpha_v\beta_3$ receptor supports the hypothesis that a putative I-like domain conformation in β_3 is incompatible with the bimolecular interactions identified in our studies.

EXPERIMENTAL PROCEDURES

Materials. All amino acid derivatives and peptide synthesis reagents were purchased from PE-Biosystems (Framingham, MA). Tris(2-carboxyethyl)phosphine (TCEP) was obtained from Pierce (Rockford, IL). Na^{125}I was from Amersham-Pharmacia (Arlington Heights, IL). Endoproteinase Lys-C, endoproteinase Glu-C, and endoglycosidase F/N-glycosidase F were from Roche Diagnostics (Indianapolis, IN). Tissue culture media were from Gibco-BRL (Gaithersburg, MD). All tissue culture disposables and plasticware were from Corning (Corning, NY). All other chemical reagents were of highest analytical grade available and were purchased from the Aldrich/Sigma/Fluka group (St. Louis, MO).

Electrospray ionization mass spectra were recorded on a Micromass Platform LCZ system equipped with an electrospray ionization source and a Waters 2690 separation module. Vydac C18 (5 μm, 300 Å, 4.6 mm × 250 mm and 10 mm × 250 mm) columns were used for analytical and preparative reversed-phase high-performance liquid chromatography (RP-HPLC); the solvent system that was used included a water/TFA mixture (1000:1, eluent A) and an acetonitrile/TFA mixture (1000:1, eluent B). Linear elution gradients were used ("Waters Gradient 6"), unless otherwise stated. Flow rates were 0.2 mL/min for analytical and 20 mL/min for preparative RP-HPLC, and samples were monitored at 220 and 254 nm.

Synthesis of [Arg^{35},Lys^{45}(N^{ϵ}-pBz_2)]Echistatin [K^{45}(BP)]. The linear precursor of the echistatin analogue was synthesized by automated solid-phase methodology on an Applied Biosystems 430A peptide synthesizer using Boc/HOBt/DCC

[1] Abbreviations: Acm, acetamidomethyl; Boc, *tert*-butyloxycarbonyl; BNPS-skatole, 3-bromo-3-methyl-2-(2-nitrophenylmercapto)-3*H*-indole; BP, benzophenone; Bpa, *p*-benzoylphenylalanyl; DCC, *N*,*N*′-dicyclohexylcarbodiimide; DTT, dithiothreitol; EDTA, ethylenediaminetetraacetic acid; Endo-F, endoglycosidase-F/N-glycosidase F; ESI-MS, electrospray ionization mass spectroscopy; Glu-C, endoproteinase Glu-C; HEK, human embryonic kidney; HOBt, 1-hydroxybenzotriazole; Lys-C, endoproteinase Lys-C; mAb, monoclonal antibody; MIDAS, metal ion-dependent adhesion site; Msc, methoxycarbonylsulfonyl; M-PER, mammalian protein extraction kit; NMR, nuclear magnetic resonance; PAGE, polyacrylamide gel electrophoresis; PAM, *p*-(oxymethyl)phenylacetamidomethyl resin; *p*Bz_2, *p*-benzoylbenzoyl; PAS, photoaffinity scanning; PBS, phosphate-buffered saline; PEG, poly(ethylene glycol); RGD, argynyl-glycyl-aspartyl; RP-HPLC, reverse phase high-performance liquid chromatography; SDS, dodecyl sulfate sodium salt; TCEP·HCl, tris(2-carboxyethyl)phosphine hydrochloride; TFA, trifluoroacetic acid.

chemistry. The *p*Bz_2 moiety at position 45 was introduced as Boc-Lys(N^{ϵ}-*p*Bz_2)-OH, as described previously (*42*). All Cys side chains were Acm-protected, while all the other side chain functions were protected in the standard manner compatible with TFA deprotection of N^{α}-Boc groups prior to stepwise elongation and liquid HF deprotection of side chain protecting groups (except the *S*-Acm) and concomitant cleavage from the resin. The peptide was assembled on 0.12 mmol of Boc-Thr(Bzl)-PAM resin (loading, 0.7 mmol/g). Residues were incorporated by a double-coupling protocol (2 mmol per cycle) followed by a capping step with acetic anhydride. The quality of the individual coupling steps was periodically monitored by the Kaiser test (*43*). Liquid HF in the presence of 10% anisole at 0 °C cleaved the product from the resin. The resin/crude peptide mixture was precipited and washed with ether. The crude peptide was dissolved in 50% acetic acid and purified by RP-HPLC (linear gradient from 0 to 50% B in A over the course of 120 min) followed by removal of the acetonitrile in vacuo and lyophilization of the aqueous solution. The pure linear and *S*-Acm protected K^{45}(BP) was characterized. ESI-MS: MW calcd 6230, found 1039 [(M + $6H^+$)/6], 1247 [(M + $5H^+$)/5], 1558 [(M + $4H^+$)/4], 2078 [(M + $3H^+$)/3]. Analytical RP-HPLC: t_R = 18.5 min, linear gradient from 0 to 60% B in A over the course of 30 min.

The purified partially protected (*S*-Acm) linear precursor (50 mg, 8.1 μmol) was dissolved in a MeOH/water mixture (2:1, v/v, 2 mL), and methoxycarbonylsulfonyl chloride (200 μL, 1.5 mmol) was added under ice cooling (*44*). After 15 min, the entire solution was subjected to an RP-HPLC separation (linear gradient from 0 to 50% B over the course of 120 min). The isolated *S*-methoxycarbonylsulfonyl (*S*-Msc) protected linear precursor (42 mg, 6.6 μmol) was dissolved in water (3 mL), and tris(2-carboxyethyl)phosphine hydrochloride (TCEP·HCl) (100 mg, 0.35 mmol) was added (*45*). After 20 min, the solution was injected into the RP-HPLC system (gradient from 0 to 50% B over the course of 120 min), and the eluted product was immediately lyophilized. The reduced analogue was then dissolved in 0.07 M NH_4OAc buffer (500 mL, pH 8.0) and mixed for 24 h at 4 °C followed by mixing for 2 days at room temperature (*32*). Final purification of the oxidized material was achieved by RP-HPLC (linear gradient from 0 to 50% B over the course of 120 min), and the product was characterized by ESI-MS and amino acid analysis. ESI-MS: MW calcd 5654, found 943 [(M + $6H^+$)/6], 1132 [(M + $5H^+$)/5], 1414 [(M + $4H^+$)/4], 1886 [(M + $3H^+$)/3]. Analytical RP-HPLC: t_R = 18.49 min (linear gradient from 0 to 60% B over the course of 30 min). Amino acid analysis (found/calcd): Asx 8.8/8, Thr 2.3/3, Ser 1.5/1, Glx 3.5/3, Pro 4.1/4, Gly 5.4/5, Ala 2.1/2, Cys 6.4/8, Met 0.9/1, Ile 1.0/1, Leu 1.1/1, Tyr 0.9/1, Phe 1.1/1, His 1.0/1, Lys 3.4/3, Arg 5.2/5.

Radioiodination of [Arg^{35},Lys^{45}(N^{ϵ}-pBz_2)]Echistatin [^{125}I-K^{45}(BP)]. Radioiodination was achieved by the lactoperoxidase method as outlined elsewhere (*46*). In brief, K^{45}(BP) (70 μg, 12 nmol) was dissolved in 0.1 M NaH_2PO_4 buffer (pH 7.4, 100 μL). Lactoperoxidase (0.2 unit) in NaH_2PO_4 buffer (20 μL) was added to a solution of the peptide (50 μL) followed by 2 mCi of $Na^{125}I$ in a NaOH solution. Four aliquots (2.5 μL each) of H_2O_2 (0.003% w/v) were added every 3 min. The resulting solution was subjected to RP-HPLC purification (Waters nonlinear gradient 8 from 19 to 50% B in A over the course of 30 min). The isolated radioactive peak was used for the photoaffinity cross-linking experiment without further treatment.

Competition Binding Assay. The binding properties of K^{45}(BP) for the purified $\alpha_v\beta_3$ receptor were assessed as described elsewhere (*47*).

Photoaffinity Cross-Linking to HEK293 Cells Over-expressing Human Integrin $\alpha_v\beta_3$. Radiolabeled K^{45}(BP) [^{125}I-K^{45}(BP)] (~10^8 cpm, ~20 pmol) was cross-linked to confluent HEK293 cells stably expressing recombinant human integrin $\alpha_v\beta_3$ (~10^6 copies/cell) (ten 75 cm^2 plates, ~9 nmol of $\alpha_v\beta_3$ receptor) according to a published protocol (*21*). Following cross-linking, the cells were washed three times with phosphate-buffered saline (PBS) and lysed by incubation for 30 min with M-PER (10 mL) (Pierce), and the ligand−receptor photoconjugate was purified by preparative SDS−PAGE after reduction with dithiothreitol (DTT) and alkylation of Cys residues with iodoacetamide, as described elsewhere (*48*). S-Pegylation was achieved by adding a 100 mM *O*-(2-maleimidoethyl)-*O*′-methylpoly-(ethylene glycol) 5000 (Fluka, Milwaukee, WI) (100 μL) solution to the reduced ligand−receptor conjugate.

Enzymatic and Chemical Digestions of the Ligand-Conjugated Receptor. Enzymatic and chemical digestions were performed according to the protocols published by Bisello et al. (*48*) and Bitan et al. (*27*).

Molecular Modeling. The construction of the molecular model is described in detail elsewhere (*27*). In brief, the amino acid sequence of β_3[99−300] was constructed using a home-written distance geometry program, which was then fitted onto the structural features of the I domain α_M using template forcing. The sequence homology that was employed was the one suggested by Tozer et al. (*49*). The resulting model was then relaxed (energy-minimized) and refined using the CVFF91 force field module within the Discover program (Molecular Simulations, Inc., San Diego, CA).

RESULTS

Design and Synthesis of the BP-Containing Echistatin Analogue. The purity of the echistatin analogue, [Arg^{35},Lys^{45}-(N^{ϵ}-pBz_2)]echistatin [K^{45}(BP)], exceeded 95% as determined by analytical RP-HPLC, and its structural integrity was established by amino acid analysis and ESI-MS. The ϵ-amino group on lysyl in position 45 is substituted with the BP photophore. In addition, Lys^{35} located in the rigid core of echistatin is substituted with Arg (*36*). This substitution was introduced to render the ligand portion of the ligand−receptor photoconjugate stable toward endopeptidase Lys-C (Lys-C), thus maintaining the structural connectivity between Lys^{45}, the residue carrying the photophore, and Tyr^{31}, the residue tagged by radioiodine. This connectivity is essential for monitoring the biochemical analysis aimed at the identification of the contact site. The biochemical analysis employs several primary and secondary chemical and enzymatic digestions to identify the minimal receptor sequence that contains the site of contact to Lys^{45} in echistatin (vide infra).

All Cys residues were side chain protected by the HF resistant acetamidomethyl (Acm) group. To maintain the structural integrity of the BP moiety, during HF deprotection of side chains and concomitant cleavage from resin, we avoided the use of any thiol-containing scavengers (*50*). The replacement of the Acm protecting group with the more labile

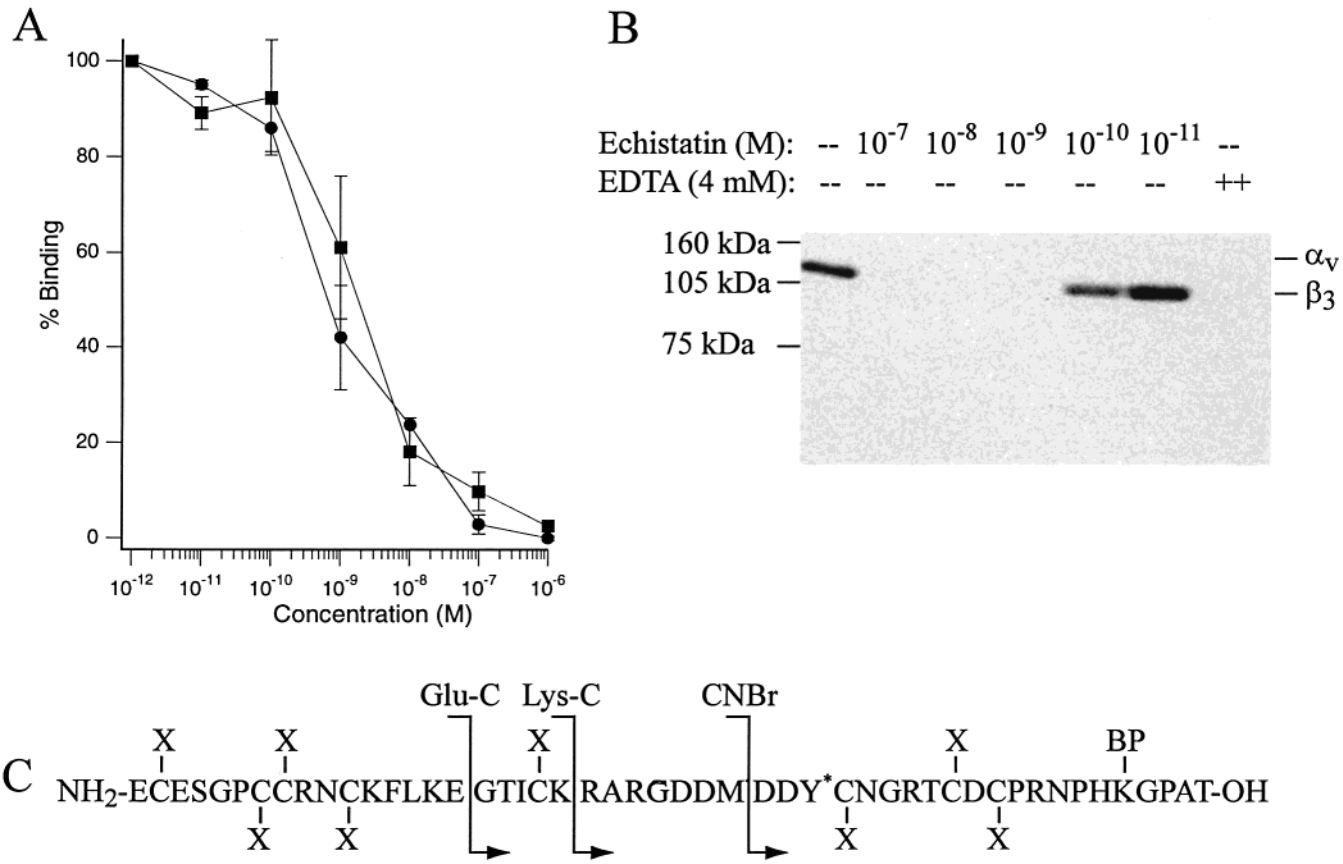

Enzyme / Chemical	X = H	X = CH_2-$COONH_2$	X = PEG(5000)
none/BNPS-Skatole	5785 Da	6244 Da	~46 kDa
Glu-C	3957 Da	4185 Da	~24 kDa
Lys-C	3453 Da	3623 Da	~19 kDa
CNBr	2652 Da	2822 Da	~18 kDa

FIGURE 1: Characterization of [Arg^{35},Lys^{45}(N^{ϵ}-$p$$Bz_2$)]echistatin. (A) Competition curves for binding of echistatin (●) and [Arg^{35},Lys^{45}(N^{ϵ}-$p$$Bz_2$)]echistatin (■) to $\alpha_v\beta_3$ receptors. ^{125}I-labeled echistatin was used as a tracer. Each result that is shown represents three independent experiments performed in duplicate. (B) Inhibition of cross-linking ^{125}I-[Arg^{35},Lys^{45}(N^{ϵ}-$p$$Bz_2$)]echistatin [^{125}I-$K^{45}$(BP)] to HEK293 cells overexpressing the $\alpha_v\beta_3$ receptor by competing with echistatin or by addition of EDTA. Samples were analyzed by 7.5% SDS−PAGE followed by autoradiography. The autoradiograph is representative of three reproducible independent experiments. Molecular mass markers are shown on the left side of the autoradiograph. (C) Primary amino acid sequence of echistatin. The asterisk depicts the site of radioiodination. The peptide bonds susceptible to enzymatic and/or chemical cleavage generating the radio- and photoreactive fragment are shown. The table depicts the molecular masses of the corresponding reduced and/or alkylated fragments.

methoxycarbonylsulfonyl (Msc) group was introduced to avoid the direct deprotection of Acm, which employs chemistry which is not tolerated by the BP moiety. Interestingly, despite the numerous structural modifications introduced into the native sequence of echistatin, the linear precursor of K^{45}(BP) folded spontaneously during the oxidation to generate a major product of the correct molecular mass, which maintained a high affinity of binding to the $\alpha_v\beta_3$ receptor (vide infra). We therefore assume that the pattern of the four disulfide bonds in K^{45}(BP) is identical to the one in the native echistatin, which was folded under the same oxidation procedure (*38*).

Biological Characterization of K^{45}(BP). The binding affinity of the echistatin analogue K^{45}(BP) for the human recombinant $\alpha_v\beta_3$ receptor was evaluated by a competition binding assay using purified and radioiodinated native echistatin as a tracer (*47*). The side chain modification of Lys^{45} with $p$$Bz_2$ and the Lys^{35} to Arg substitution decreased the binding affinity only 3-fold compared to that of the parent compound ($IC_{50} = 6 \times 10^{-10}$ and 2×10^{-9} M, respectively) (Figure 1A). None of the radioiodinated echistatin analogues bound significantly to nontransfected HEK293 cells (results not shown).

Photoaffinity Cross-Linking. ^{125}I-K^{45}(BP) was generated by radioiodination of K^{45}(BP) employing the lactoperoxidase method (*46*). ^{125}I-K^{45}(BP) was incubated with HEK293 cells stably expressing the recombinant human $\alpha_v\beta_3$ receptor (~10^6 receptors/cell) (*21*). Upon irradiation at 365 nm, the photoreactive ^{125}I-K^{45}(BP) analogue cross-linked with high efficiency almost exclusively to the β_3 subunit, as shown by

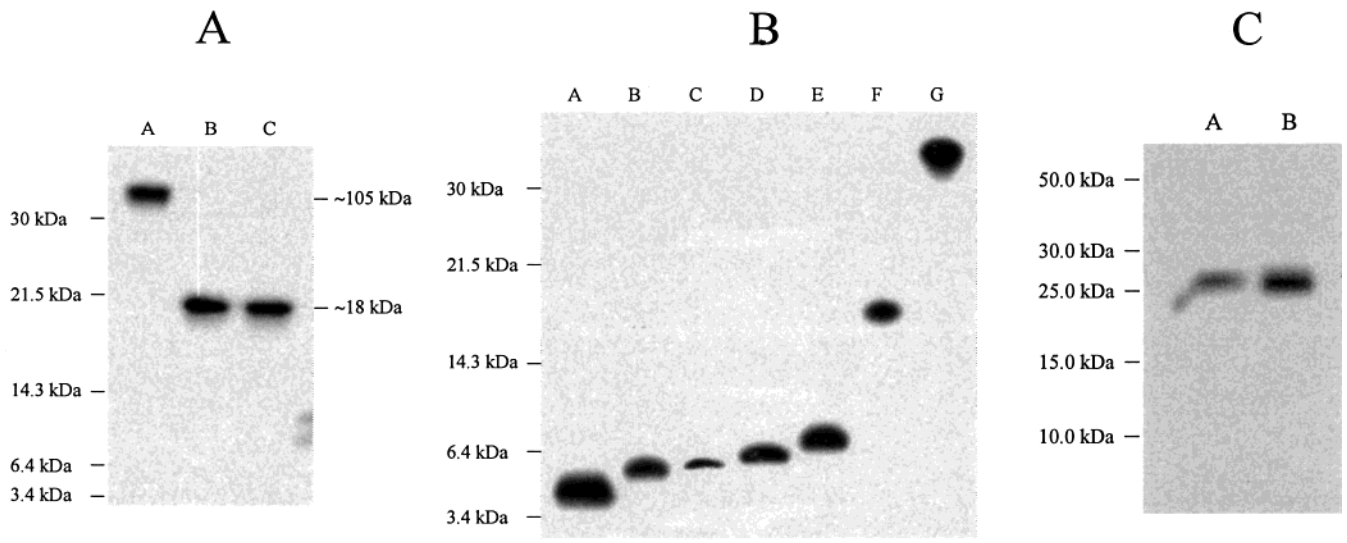

FIGURE 2: Autoradiographs of the ^{125}I-[Arg^{35},Lys^{45}(N^{ϵ}-*p*Bz$_2$)]-echistatin−β_3 photoconjugate by SDS−PAGE. (A) Primary digestion pattern of the ^{125}I-[Arg^{35},Lys^{45}(N^{ϵ}-*p*Bz$_2$)]echistatin−β_3 [^{125}I-K^{45}(BP)−β_3] conjugate by BNPS-skatole and secondary digestion of the BNPS-skatole-generated band by endoglycosidase F: lane A, ^{125}I-K^{45}(BP)−β_3 conjugate (∼105 kDa); lane B, BNPS-skatole fragment (∼18 kDa); and lane C, BNPS-skatole (1) and Endo-F fragment (∼18 kDa) (2). No deglycoslylation can be observed, indicating the generation of a nonglycosylated fragment by BNPS-skatole (16.5% Tricine gel). (B) Pattern of digestion of the ^{125}I-K^{45}(BP)−β_3 conjugate by BNPS-skatole (lane F), CNBr (lane E), endoproteinase Lys-C (lane D), and endoproteinase Glu-C (lane B). Reduced (but not alkylated) forms of ^{125}I-[Arg^{35},Lys^{45}(*p*Bz$_2$)]echistatin undigested or digested with endoproteinase Glu-C (lanes C and A, respectively) serve as internal markers of molecular masses (5.7 and 4.0 kDa, respectively) (16.5% Tricine gel). (C) Pattern of digestion of the ^{125}I-[Arg^{35},Lys^{45}(N^{ϵ}-*p*Bz$_2$)]echistatin−β_3 [^{125}I-K^{45}(BP)−β_3] conjugate reduced and alkylated with *O*-(2-maleimidoethyl)-*O*′-methylpoly(ethylene glycol) 5000 by endoproteinase Glu-C (lane A) and endoproteinase Lys-C (lane B). Alkylation with *O*-(2-maleimidoethyl)-*O*′-methylpoly(ethylene glycol) 5000 adds 5 kDa per cysteine residue in the fragment. This provides a means of distinguishing between fragments of similar size but with different numbers of cysteine residues by SDS−PAGE analysis. These autoradiographs are representative of three reproducible independent experiments. The molecular mass markers are indicated on the left side of the autoradiographs.

SDS−PAGE (band at ∼105 kDa, Figure 1B). Furthermore, the photoinsertion of ^{125}I-K^{45}(BP) into the β_3 subunit was competitively inhibited by native echistatin in a dose-dependent manner, reflecting the specificity of the cross-linking process (Figure 1B). No cross-linking was observed in the presence of 4 mM EDTA, consistent with the ligand−receptor interaction known to be Ca^{2+} and Mg^{2+} ion-dependent (Figure 1B) (*51*).

Identification of the Contact Domain between ^{125}I-K^{45}(BP) and $\alpha_v\beta_3$. Following irradiation with UV light, the cells were solubilized and the ^{125}I-K^{45}(BP)−β_3 photoconjugate was reduced, alkylated with iodoacetamide, and isolated by preparative SDS−PAGE. It was then subjected to a series of chemical and enzymatic digestions using BNPS-skatole, cyanogen bromide (CNBr), endoproteinase Lys-C (Lys-C), and endoproteinase Glu-C (Glu-C). Native echistatin contains CNBr-, Lys-C-, and Glu-C-susceptible peptide bonds (Met^{28}, Lys^{12,15,21,35}, and Glu^{1,3,16}, respectively). Substitution of Lys^{35} with Arg prevents Lys-C-mediated cleavage separating the radioactive tag (incorporated at Tyr^{31}) from the photoreactive moiety (N^{ϵ}-*p*Bz$_2$-modified Lys^{45}) during fragmentation and analysis of the photoconjugate. The cleavage pattern of these chemicals and/or enzymes and the molecular masses of the radioactive and photoreactive ligand fragments in the alkylated and nonalkylated form are depicted in Figure 1C.

Digestion of the intact ^{125}I-K^{45}(BP)−β_3 photoconjugate (Figure 2A, lane A) by BNPS-skatole (cleaving primarily at the carboxyl side of Trp) generated a single radiolabeled band with an apparent molecular mass of ∼18 kDa (Figure 2A, lane B). Isolation of this band and subsequent treatment with endoglycosidase F/N-glycosidase F (Endo F) did not alter the electrophoretic mobility (Figure 2A, lane C), demonstrating the lack of N-glycosylation sites within the BNPS-skatole-generated fragment (Figure 2A). Analysis of the theoretical BNPS-skatole digestion map of the β_3 subunit identifies two candidate fragments, β_3[130−238] and β_3[477−553] (Figure 3). Neither fragment contains a potential N-glycosylation site. The molecular masses of the potential photoconjugates are 18.6 and 16.8 kDa, respectively (Figure 4). This small difference in molecular mass cannot be resolved by SDS−PAGE, precluding unambiguous assignment of the contact domain to one of the two fragments.

A second independent digestion involved CNBr-mediated cleavage, breaking peptide bonds at the carboxyl side of Met residues. Treatment of the intact ligand−β_3 photoconjugate (∼105 kDa) with CNBr produces a radioactive band that migrates more slowly than the band of the reduced and undigested radioiodinated ligand ^{125}I-K^{45}(BP) (5785 Da) and slightly above the 6.4 kDa molecular mass marker (Figure 2B, lane E). This result excludes one of the above-mentioned possible BNPS-skatole fragments β_3[477−553], since all possible CNBr-generated fragments overlapping this domain would have molecular masses distinctively higher (>10 kDa) than the observed one (Figure 2B, lane E). However, cross-linking to the putative CNBr-generated fragment β_3[188−227], which lies entirely within the BNPS-skatole fragment β_3[130−238], yields a photoconjugated fragment [^{125}I-K^{45}(BP)(30−49)−β_3[188−227]] of the appropriate molecular mass (7.4 kDa). Indeed, this fragment is unique within the entire β_3 subunit, since all other possible CNBr-generated fragments of the ^{125}I-K^{45}(BP)−β_3 conjugate would have molecular masses well above or below 7.4 kDa.

Treatment of the isolated ^{125}I-K^{45}(BP)−β_3 photoconjugate with Lys-C resulted in a radioactive band (∼6.2 kDa) mi-

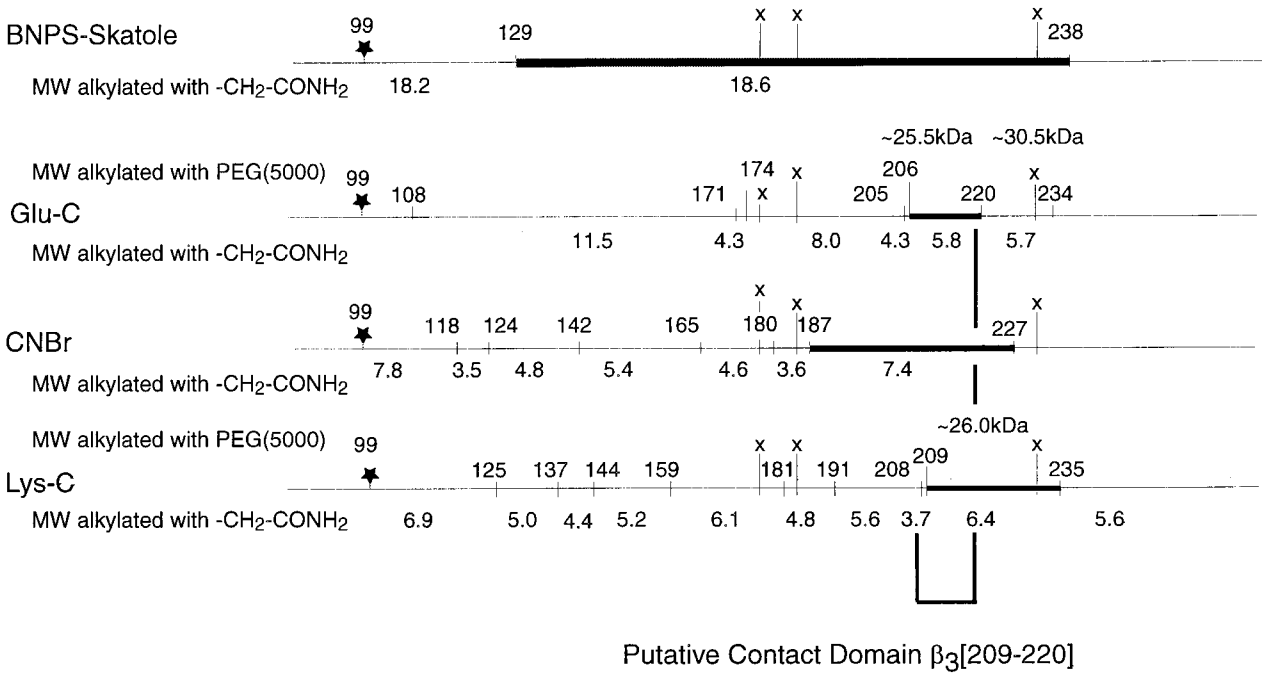

FIGURE 3: Predicted digestion map of the region of residues 95−250 of the β_3 chain. Cleavage points are shown for BNPS-skatole, CNBr, and endoproteinases Lys-C and Glu-C. The expected molecular mass of the ^{125}I-K^{45}(BP)−β_3 fragment is indicated. Numbers below the sequence represent expected masses for fragments alkylated with iodoacetamide (in kilodaltons), while numbers above the sequence represent molecular masses of fragments alkylated with *O*-(2-maleimidoethyl)-*O*′-methylpoly(ethylene glycol) 5000. The domains identified in the cleavage paths that were used are highlighted in bold lines (see the text and Figure 2). The stars represent potential glycosylation sites, and the x's denote cysteine residues.

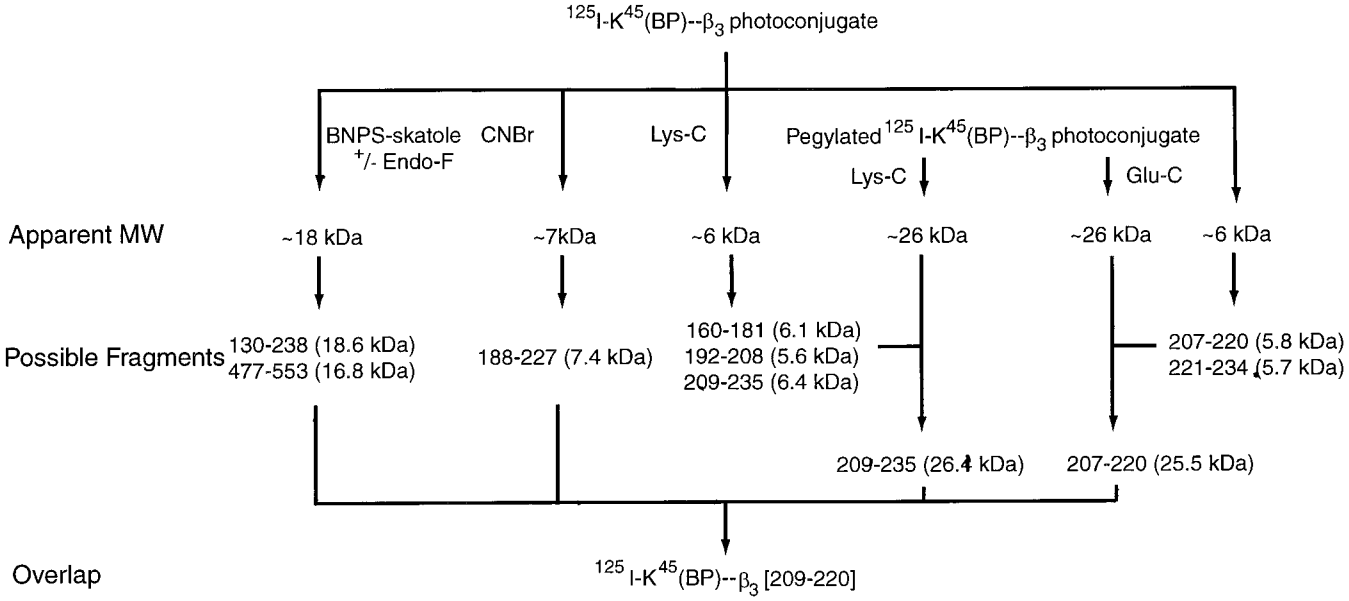

FIGURE 4: Schematic summary of the fragmentation results of the reduced and alkylated (with iodoacetamide) ^{125}I-K^{45}(BP)−β_3 photoconjugate and its reduced and pegylated form. Ambiguous fragmentation products that cannot be resolved by SDS−PAGE analysis are listed under the corresponding cleavage pathways.

grating marginally above the radioactive ligand ^{125}I-K^{45}(BP) (5785 Da) (Figure 2B, lanes D and C, respectively). Within the putative BNPS-skatole-generated conjugated fragment ^{125}I-K^{45}(BP)−β_3[130−238], only three potential Lys-C-generated conjugated fragments [^{125}I-K^{45}(BP)(22−49)−β_3[160−181], −β_3[192−208], and −β_3[210−235]] have molecular masses similar to that of the observed Lys-C-generated band. Furthermore, only the sequences of the two conjugated fragments corresponding to β_3[192−208] and β_3-[210−235] overlap with the sequences of the CNBr- and BNPS-skatole-generated fragments (Figures 3 and 4). Their alkylated forms correspond to molecular masses of 5.6 and 6.4 kDa, respectively. Since the radioactive band appears to migrate marginally above the radioactive ligand ^{125}I-K^{45}(BP) (5785 Da), the evidence favors the larger conjugated fragment corresponding to β_3[210−235] (6.4 kDa) being the putative Lys-C-generated conjugated fragment containing the photoinsertion site. However, due to the limited resolution of SDS−PAGE analysis, the radioactive band cannot be unambiguously assigned to this fragment of the photoconjugate.

Nevertheless, the different number of cysteine residues present in the two possible fragments can be exploited to

distinguish them. The larger Lys-C-generated conjugated fragment, corresponding to β_3[210−235], contains four cysteine residues [three in the ligand portion ($Cys^{32,37,39}$) and one in the receptor fragment (Cys^{232})]. The conjugated fragment corresponding to β_3[192−208] contains only the three cysteine residues located in the Lys-C-generated photoreactive portion of echistatin (Figure 1C). Therefore, we alkylated the reduced ^{125}I-K^{45}(BP)−β_3 conjugate with a PEG-5000-maleimide, a thiol-specific reagent, and subsequently subjected the pegylated conjugate to Lys-C digestion. The anticipated molecular masses of the two possible pegylated Lys-C-generated photoconjugated fragments, corresponding to the ^{125}I-K^{45}(BP)(22−49)−β_3[192−208](PEG-5000)$_3$ and ^{125}I-K^{45}(BP)(22−49)−β_3[210−235](PEG-5000)$_4$ photoconjugate fragments, are shifted from 5.6 and 6.4 kDa in the acetamidated forms to 20.6 and 26.4 kDa in the pegylated forms, respectively. This shift and resulting difference in molecular mass of ∼6 kDa can be easily detected by SDS−PAGE analysis. As shown in Figure 2C (lane B), we observe a band at ∼26 kDa and therefore assign unambiguously the photoinsertion site as being within β_3[210−235] (Figure 4). However, photo-cross-linking to Lys^{209}, a potential insertion site, cannot be excluded. In that event, Lys-C would no longer hydrolyze the peptide bond between Lys^{209} and Gln^{210} but would cleave the bond between the two adjacent lysine residues in positions 208 and 209, leading to a different Lys-C-generated fragment, which includes β_3[209−235]. The resolution of SDS−PAGE analysis does not rule out this possibility. Therefore, we must expand the boundaries of the Lys-C-generated conjugated fragment containing the site of contact to β_3[209−235]. Taken together, with the results obtained from the BNPS-skatole, CNBr, and Lys-C protein digest mapping, we can identify β_3[209−227] as the minimal putative contact domain generated by the restriction cleavages of Lys-C and CNBr at Lys^{208} and Met^{227}, respectively (Figure 3).

To further delineate the 19-amino acid sequence containing the contact site, we carried out a Glu-C digestion on the intact, reduced, and alkylated ^{125}I-K^{45}(BP)−β_3 conjugate. The radioactive conjugated fragment observed at ∼5.5 kDa (Figure 2B, lane B) may correspond to one of two possible sequences, β_3[207−220] and β_3[221−234], both overlapping the CNBr/Lys-C-restricted, minimal putative contact domain β_3[209−227] (Figure 3). The calculated molecular masses of these two potential photoconjugated fragments cannot be distinguished by SDS−PAGE analysis (5.8 and 5.7 kDa, respectively). Once again, the different number of cysteine residues (4 vs 5, respectively) in the two possible fragments provides the means of distinguishing between them. The anticipated molecular mass of the possible ^{125}I-K^{45}(BP)(17−49)−β_3[207−220] photoconjugated fragment is shifted upon pegylation from 5.8 to ∼25.5 kDa [^{125}I-K^{45}(BP)-(17−49)−β_3[207−220](PEG-5000)$_4$] and for the ^{125}I-K^{45}(BP)-(17−49)−β_3[221−234] fragment from 5.7 to ∼30.5 kDa [^{125}I-K^{45}(BP)(17−49)−β_3[221−234](PEG-5000)$_5$] (Figure 4). As shown in Figure 2C (lane A), digestion of the PEG-5000-alkylated ^{125}I-K^{45}(BP)−β_3 conjugate with Glu-C results in a radioactive fragment migrating with an apparent molecular mass of ∼26 kDa, thus corresponding to the pegylated conjugate derived from the β_3[207−220] fragment. We can therefore further delineate the minimal putative sequence containing the site of contact to β_3[209−220]. This sequence is restricted by the cleavage sites of Lys-C and Glu-C at Lys^{208} and Glu^{220}, respectively (Figure 3). This sequence of 12 amino acids from the β_3 subunit in the $\alpha_v\beta_3$ receptor is the contact site for the photophore-bearing Lys^{45} located at the C-terminus of echistatin.

DISCUSSION

Understanding the bimolecular interactions between integrins and their ligands is of fundamental importance for elucidating the molecular mechanism of ligand recognition and specificity, and signal transduction. However, the powerful tools of high-resolution structural analysis, such as X-ray crystallography and NMR, are not available for studies of intact integrin $\alpha\beta$ heterodimers due to their size and nature as membrane-embedded proteins. Structural studies of integrins depend, therefore, on techniques which deliver low-resolution structural data (*11*, *12*, *15*−*20*, *52*, *53*). Mutational analysis reveals important residues for integrin functionality within both the α and β subunits (*13*, *14*, *54*). On the basis of low-resolution techniques taken in combination with molecular modeling approaches, the α subunits are predicted to fold into a seven-bladed "β propeller" (*55*). However, significant controversy is found in predictions of the structure of β subunits (*13*, *56*, *57*). On the basis of similarities in the hydrophobicity profile and homology analysis, Lee and co-workers predicted that the large region around β_3[100−300] adopts a dinucleotide binding fold, as found in inserted domains (I domains) of many α subunits but not in α_v (*57*). Nevertheless, different methods of sequence alignment used in combination with distinct X-ray structures as templates result in significantly different models (*27*). Therefore, experimental evidence is needed to validate and/or refine models of the β subunit.

Such evidence can be gained by the photoaffinity scanning approach that can identify residues involved in the ligand−receptor bimolecular interface. These "contact domains", which are part of the ligand-binding sites (or surface), combined with structural information about the ligand, generate valuable insights for building an experimentally supported model of the ligand−integrin complex (*29*, *30*, *33*). Here we report the identification of a contact domain between the β_3 subunit in the $\alpha_v\beta_3$ receptor and the C-terminus of echistatin.

Echistatin displays high affinity toward the $\alpha_v\beta_3$ and $\alpha_{IIb}\beta_3$ integrin receptors. Its RGD triad is located in the mobile loop at the tip of the hairpin and has been shown to be important for irreversible binding to the $\alpha_v\beta_3$ receptor (*38*, *39*). The flexible C-terminal part of echistatin has been shown to contribute further to integrin binding affinity. However, the spatial relation between binding sites, for the RGD triad and the C-terminal domain of echistatin, on the $\alpha_v\beta_3$ receptor is not clear. This photoaffinity cross-linking study was designed (i) to determine whether there is experimental evidence for a binding site within the $\alpha_v\beta_3$ integrin which accommodates the non-RGD auxiliary receptor binding domain located at the C-terminal part of echistatin and (ii) to expand the pool of available experimental data to support a structural model of the ligand−$\alpha_v\beta_3$ receptor binding interface.

For this photoaffinity cross-linking study, we designed and synthesized the full-length ^{125}I-K^{45}(BP) analogue. After generation and isolation of the ^{125}I-K^{45}(BP)−β_3 photocon-

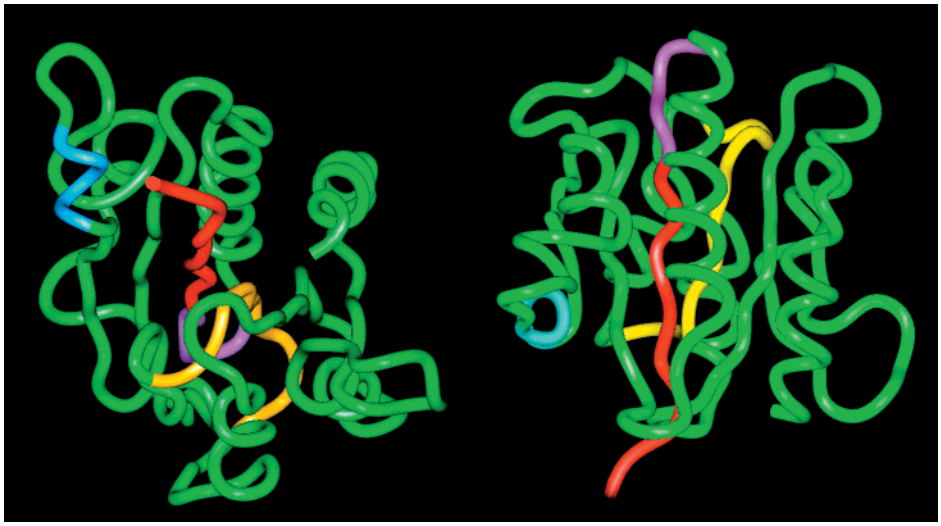

FIGURE 5: Two views (rotated 90°) of a molecular model of the β_3 I-like domain β_3[99−300] based on homology modeling and the β_3 I domain as a template. Pink represents the MIDAS motif (β_3[119−123]), red the RGD-contact domain β_3[99−118] previously reported in ref *21*, blue the RGD-contact domain β_3[167−171] previously reported in ref *27*, and yellow the minimal putative contact site in the β_3 subunit (β_3[209−220]), for Lys^{45} in echistatin.

jugate, by chemical and enzymatic techniques, a fragment of 12 residues, β_3[209−220], was identified as the contact site for residue 45 located at the C-terminus of echistatin (Figures 3 and 4). Interestingly, the nearly identical amino acid segment β_3[211−222] has been shown to block the binding of fibrinogen to $\alpha_{IIb}\beta_3$ (*58*). Furthermore, the peptide β_3[217−231] interacts with fibrinogen (which has a sequence significantly homologous with the C-terminal domain of echistatin) in an RGD-independent manner (*59*). In addition, the naturally occurring mutation of Arg^{214} to Gln within this domain inhibits fibrinogen binding and causes a variant form of Glanzmann's thrombasthenia (*60*). Finally, Tozer and co-workers identified Asp^{217} in β_3 as an essential residue for ligand binding and function of the $\alpha_{IIb}\beta_3$ receptor and proposed this residue to be part of the MIDAS motif (*49*). Later, Lin et al. supported this proposal by showing that the mutation of Asp^{217} to Ala in β_3 diminishes the apparent affinity of Mn^{2+} for $\alpha_{IIb}\beta_3$ by 15−20-fold (*13*). Taken together, these reports attribute functional significance to sequences and amino acid residues within β_3[209−220], the minimal echistatin's C-terminal binding domain, and highlight the importance of it as a contact domain.

On the basis of sequence homology and similarity in the hydrophobicity profile between I domains and portions of the β_3 subunit, we and others have developed different models for this I domain-like region (*27*, *49*). The model reported by Tozer et al. (*49*) and one of our models (*27*) are based on homology modeling using the crystal structure of the α_M I domain as a template. This model predicts that the contact domain β_3[209−220] is a portion of a β strand, mostly buried in the core of the I-like domain (residues 109−352). In this case, only the N- and C-terminal parts of this domain are accessible for cross-linking, while photoinsertion into the midregion would be sterically hindered (Figure 5). Our second model (*27*), which is based on the crystal structure of the α_2 I domain and a different homology alignment, predicts that the contact domain β_3[209−220] is located in an entirely accessible loop on the opposite side of the MIDAS motif (not shown). However, only the α_M-related model is in full agreement with the above-mentioned role of residues Asp^{217} and Glu^{220} in metal coordination. We therefore focus on the α_M-related model for the interpretation of our cross-linking data.

In the model based on the α_M I domain, the accessible N-terminal part of the contact domain β_3[209−220] is on the opposite side of the MIDAS motif and is slightly covered by a poorly defined loop. Additionally, in two previous cross-linking studies with small cyclic RGD-containing peptides, we identified the sequences β_3[99−118] (*21*) and β_3[167−171] (*27*) as being in direct contact with residues flanking either side of the RGD motif. We concluded in the latter report that a direct interaction between the RGD-containing ligand and the MIDAS motif is unlikely, since the RGD contact surface is located on the opposite side of the MIDAS motif in both models. The identification of β_3[209−220] as a contact domain for Lys^{45} in echistatin further supports our proposal. However, we are aware of several studies that conclude that many receptors adopting a dinucleotide fold bind their ligands at the "MIDAS face" (*61*). Furthermore, it is proposed that the interface between the α_M I domain and the rest of the α_M subunit is formed by residues located opposite the MIDAS motif (*55*). Hence, the proposed ligand-binding surface would overlap with the surface involved in the interaction with the rest of the β_3 subunit and is therefore unlikely to be accessible to the ligand.

Evidently, the accessible C-terminal portion of the contact domain β_3[209−220] offers no alternative explanation. Cross-linking of ^{125}I-K^{45}(BP) to this accessible side would impose an energetically unfavorable distortion of the rigid core structure (imposing an extended conformation of the peptide and distorted bonds) of echistatin since the RGD motif would have to interact with domains located on the opposite face of the β_3[99−330] domain. Consequently, such a spatial arrangement would result in an energetically unfavorable conformation of echistatin and would translate into low-affinity binding, which is not observed.

The conclusion drawn from our cumulative cross-linking data, consistent with data from other methods, is either (i) a lack of an I domain-like fold in the β_3 subunit of the $\alpha_v\beta_3$ receptor or (ii) a lack of an I domain-like fold only in the

ligand-bound conformation of the β_3 subunit of $\alpha_v\beta_3$. The last possibility implies the occurrence of a major conformational change in the I-like domain upon ligand binding. The absence of an I domain-like fold in the β_3 and β_5 subunits as suggested by Lin et al. supports the general importance of a MIDAS motif for ligand binding (*13*).

Binding of echistatin and vitronectin to $\alpha_v\beta_3$ has been reported previously to be irreversible (*62*, *63*). The interaction involves an initial, RGD-dependent and fully reversible integrin−ligand recognition event, followed by the stabilization of the integrin−ligand complex, leading finally to a nondissociable complex. It is suggested that this stabilized interaction between the receptor and ligand may be necessary for the transduction of signals between the extracellular matrix and intracellular compartments. This pattern of ligand binding is in agreement with the occurrence of a conformational change within $\alpha_v\beta_3$ upon ligand binding. This ligand-bound conformation may differ from the I domain-like conformation in the nonoccupied receptor. Like most mutagenesis studies, our cross-linking experiments probe the interaction between echistatin and $\alpha_v\beta_3$ at equilibrium, which is apparently reached after an extended incubation time. Assuming that the low- and high-affinity states of the receptor (*64*) represent two different conformations (*65*), our photoinsertion can therefore occur at residues which are accessible to the ligand only at the high-affinity state. According to our modeling, these residues are inaccessible to the lignd at the β I domain-like conformation.

The recently determined crystal structure of a complex between the α_2 I domain, from $\alpha_2\beta_1$ integrin, and a triple-helical collagen I-derived peptide revealed that ligand binding forces a rearrangement in the coordination sphere of the MIDAS (*65*). On the basis of these findings, Shimaoka and co-workers designed a mutant Mac-1 I domain stabilized in the open, high-affinity conformation (*66*), thus confirming that conformational changes in the I domain are relevant to the regulation of ligand binding activity that transforms the integrin from the closed (low-affinity) to the open (high-affinity) conformations. These subtle changes in the metal coordination are propagated to the rest of the integrin, leading to the outside-in signaling. Analogously, binding of an RGD peptide to the β subunit I-like domain (*67*) may lead to a conformational transformation that has functional consequences similar to those reported for the α_2 I domain (*68*). Recently, studying the interactions of mAb with the β_2 integrin subunit, Huang and co-workers suggested a structure sequence alignment and a model for the I-like domain in which the α_1 and α_6 helices are highly exposed to the solvent and may be part of the putative ligand-binding site (*69*). However, their sequence alignment and assignment of secondary structure elements are similar to those of Tuckwell and Humphries (*56*) and differ extensively from those of Tozer and co-workers (*49*) adapted in this study.

In summary, we provide direct experimental evidence which shows that the C-termial region of echistatin binds to a site within the β_3 subunit of the $\alpha_v\beta_3$ receptor, which is distinct from the sites that bind residues flanking the RGD triad in small peptide ligands. Taken together, the collective photoaffinity data obtained with three different ligands (*21*, *27*) (and this report), the reported mutagenesis studies, and the binding properties of echistatin favor the presence of a different fold in the ligand−$\alpha_v\beta_3$ receptor complex.

We now plan to continue and use the PAS approach to further characterize the echistatin−$\alpha_v\beta_3$ receptor bimolecular interface proximal to the RGD-bearing loop. This effort should eventually produce a detailed topological map of the $\alpha_v\beta_3$ residues involved in the ligand-binding surface.

REFERENCES

1. Hynes, R. O. (1992) *Cell 69*, 11−25.
2. Lakkakorpi, R., Horton, M. A., Helfrich, M. H., Karhukorpi, E.-K., and Vaananen, H. K. (1991) *J. Cell Biol. 115*, 1179−1186.
3. Horton, M. A., Taylor, M. L., Arnett, T. R., and Helfrich, M. H. (1991) *Exp. Cell Res. 195*, 368−375.
4. Mostov, K., and Werb, Z. (1997) *Science 276*, 219−220.
5. Nesbitt, S., and Horton, M. (1997) *Science 276*, 266−269.
6. Salo, J., Lehenkari, P., Mulari, M., Metsikko, K., and Vaananen, H. K. (1997) *Science 276*, 270−273.
7. Fisher, J. E., Caulfield, M. P., Sato, M., Quartuccio, H. A., Gould, R. J., Garsky, V. M., Rodan, G. A., and Rosenblatt, M. (1993) *Endocrinology 132*, 1411−1413.
8. Engleman, V. W., Nickols, G. A., Ross, F. P., Horton, M. A., Griggs, D. W., Settle, S. L., Ruminski, P. G., and Teitelbaum, S. L. (1997) *J. Clin. Invest. 99*, 2284−2292.
9. Rodan, S. B., Duong, L. T., Duggan, M., Gentile, M. A., Fisher, J. A., Leu, C.-T., Meissner, R., Nagy, R., Seedor, J. G., Wesolowski, G., Zartman, A., Rodan, G. A., and Kimmel, D. (2000) *J. Bone Miner. Res. 15*, S225.
10. Gowen, M., Emery, J. G., and Kumar, S. (2000) *Emerging Drugs 5*, 1−43.
11. Du, X., Gu, M., Weisel, J. W., Nagaswami, C., Bennett, J. S., Bowditch, R., and Ginsberg, M. H. (1994) *J. Biol. Chem. 268*, 23087−23092.
12. Rivas, G. A., Aznarez, J. A., Usobiaga, P., Saiz, J. L., and Gonzalez-Rodriguez, J. (1991) *Eur. Biophys. J. 19*, 335−345.
13. Lin, E. C. K., Ratnikov, B. I., Tsai, P. M., Gonzalez, E. R., McDonald, S., Pelletier, A. J., and Smith, J. W. (1997) *J. Biol. Chem. 272*, 14236−14243.
14. Loftus, J. C., O'Toole, T. E., Plow, E. F., Glass, A., Frelinger, A. L., III, and Ginsberg, M. H. (1990) *Science 249*, 915−918.
15. Kamata, T., Puzon, W., and Takada, Y. (1995) *Biochem. J. 305*, 945−951.
16. Yano, S., Suzuki, K., Katoh, M., Sugita, Y., Kaku, S., Kawamura, K., and Masuho, Y. (1994) *J. Biochem. 116*, 778−786.
17. Barbas, C. F., III, Languino, L. R., and Smith, J. W. (1993) *Proc. Natl. Acad. Sci. U.S.A. 90*, 10003−10007.
18. Honda, S., Tomiyama, Y., Pelletier, A. J., Annis, D., Honda, Y., Orchekowski, R., Ruggeri, Z., and Kunicki, T. J. (1995) *J. Biol. Chem. 270*, 11947−11954.
19. D'Souza, S. E., Haas, T. A., Piotrowicz, R. S., Byers-Ward, V., McGrath, D. E., Soule, H. R., Cierniewski, C., Plow, E. F., and Smith, J. W. (1994) *Cell 79*, 659−667.
20. Pelletier, A. J., Kunicki, T., and Quaranta, V. (1996) *J. Biol. Chem. 271*, 1364−1370.
21. Bitan, G., Scheibler, L., Greenberg, Z., Rosenblatt, M., and Chorev, M. (1999) *Biochemistry 38*, 3414−3420.
22. D'Souza, S. E., Ginsberg, M. H., Burke, T. A., Lam, S. C.-T., and Plow, E. F. (1988) *Science 242*, 91−93.
23. Smith, J. W., and Cheresh, D. A. (1988) *J. Biol. Chem. 263*, 18726−18731.
24. Calvete, J. J., McLane, M. A., Stewart, G. J., and Niewiarowski, S. (1994) *Biochem. Biophys. Res. Commun. 202*, 135−140.
25. Chen, L. L., Lobb, R. R., Cuervo, J. H., Lin, K.-C., Adams, S. P., and Pepinsky, R. B. (1998) *Biochemistry 37*, 8743−8753.
26. Smith, J. W., and Cheresh, D. A. (1991) *J. Biol. Chem. 266*, 11429−11432.
27. Bitan, G., Scheibler, L., Mierke, D. F., Rosenblatt, M., and Chorev, M. (2000) *Biochemistry 39*, 11014−11023.
28. Williams, K. P., and Shoelson, S. E. (1993) *J. Biol. Chem. 268*, 5361−5364.

29. Rolz, C., Pellgrini, M., and Mierke, D. F. (1999) *Biochemistry 38*, 6397−6405.
30. Phalipou, S., Seyer, R., Cotte, N., Breton, C., Barberis, C., Hibert, M., and Mouillac, B. (1999) *J. Biol. Chem. 274*, 23316−23327.
31. Dong, M., Wang, Y., Hadac, E. M., Pinon, D. I., Holicky, E. L., and Miller, L. J. (1999) *J. Biol. Chem. 274*, 19161−19167.
32. Dong, M., Asmann, Y. W., Zang, M., Pinon, D. I., and Miller, L. J. (2000) *J. Biol. Chem. 275*, 26032−26039.
33. Ji, Z., Hadac, E. M., Henne, R. M., Patel, S. A., Lybrand, T. P., and Miller, L. J. (1997) *J. Biol. Chem. 272*, 24393−24401.
34. Leitinger, B., and Hogg, N. (2000) *Nat. Struct. Biol. 7*, 614−616.
35. Gan, Z.-R., Gould, R. J., Jacobs, J. W., Friedman, P. A., and Polokoff, M. A. (1988) *J. Biol. Chem. 263*, 19827−19832.
36. Atkinson, R. A., Saudek, V., and Pelton, J. T. (1994) *Int. J. Pept. Protein Res. 43*, 563−572.
37. Saudek, V., Atkinson, R. A., and Pelton, J. T. (1991) *Biochemistry 30*, 7369−7372.
38. Garsky, V. M., Lumma, P. K., Friedinger, R. M., Pitzenberger, S. M., Randall, W. C., Veber, D. F., Gould, R. J., and Friedman, P. A. (1989) *Proc. Natl. Acad. Sci. U.S.A. 86*, 4022−4026.
39. Marcinkiewicz, C., Vijay-Kumar, S., McLane, M. A., and Niewiarowoski, S. (1997) *Blood 90*, 1565−1575.
40. Wright, P. S., Saudek, V., Owen, T. J., Harbeson, S. L., and Bitonti, A. J. (1993) *Biochem. J. 293*, 263−267.
41. Yokoyama, K., Zhang, X.-P., Medved, L., and Takada, Y. (1999) *Biochemistry 38*, 5872−5877.
42. Nakamoto, C., Behar, V., Chin, K. R., Adams, A. E., Suva, L. J., Rosenblatt, M., and Chorev, M. (1995) *Biochemistry 34*, 10546−10552.
43. Kaiser, E., Colescott, R. L., Bossinger, C. D., and Cook, P. I. (1970) *Anal. Biochem. 34*, 595−598.
44. Barany, G., Schroll, A. L., Mott, A. W., and Halsrud, D. A. (1983) *J. Org. Chem. 48*, 4750−4761.
45. Han, J. C., and Han, G. Y. (1994) *Anal. Biochem. 220*, 5−10.
46. Bolton, A. E. (1986) *Methods Enzymol. 124*, 18−29.
47. Greenberg, Z., Stoch, S., Traianedes, K., Teng, H., Rosenblatt, M., and Chorev, M. (1999) *Anal. Biochem. 266*, 153−164.
48. Bisello, A., Adams, A., Mierke, D. F., Pellegrini, M., Rosenblatt, M., Suva, L., and Chorev, M. (1998) *J. Biol. Chem. 273*, 22498−22505.
49. Tozer, E. C., Liddington, R. C., Sutcliffe, M. J., Smeeton, A. H., and Loftus, J. C. (1996) *J. Biol. Chem. 271*, 21978−21984.
50. Breslav, M., Becker, J., and Naider, F. (1997) *Tetrahedron Lett. 38*, 2219−2222.
51. Gailit, J., and Ruoslahti, E. (1988) *J. Biol. Chem. 263*, 12927−12932.
52. Kouns, W. C., Newman, P. J., Puckett, K. J., Miller, A. A., Wall, C. D., Fox, C. F., Seyer, J. M., and Jennings, L. K. (1991) *Blood 78*, 3215−3223.
53. Ni, H., and Wilkins, J. A. (1998) *Cell Adhes. Commun. 5*, 257−271.
54. Kashiwagi, H., Tomiyama, Y., Tadokoro, S., Honda, S., Shiraga, M., Mizutani, H., Handa, M., Kurata, Y., Matsuzawa, Y., and Shattil, S. J. (1999) *Blood 93*, 2559−2568.
55. Springer, T. A. (1997) *Proc. Natl. Acad. Sci. U.S.A. 94*, 65−72.
56. Tuckwell, D. S., and Humphries, M. J. (1997) *FEBS Lett. 400*, 297−303.
57. Lee, J. O., Rieu, P., Arnaout, M. A., and Liddington, R. (1995) *Cell 80*, 631−638.
58. Charo, I. F., Nannizzi, L., Phillips, D. R., Hsu, M. A., and Scarborough, R. M. (1991) *J. Biol. Chem. 266*, 1415−1421.
59. Wierzbicka, I., Kowalska, M. A., Lasz, E. C., Farrell, D. H., Budzynski, A. Z., and Niewiarowski, S. (1997) *Thromb. Res. 85*, 115−126.
60. Bajt, M. L., Ginsberg, M. H., Frelinger, A. L., Berndt, M. C., and Loftus, J. C. (1992) *J. Biol. Chem. 267*, 3789−3794.
61. Branden, C., and Tooze, J. (1999) *Introduction to Protein Structure*, 2nd ed., Garland Publishing Inc., New York.
62. Orlando, R. A., and Cheresh, D. A. (1991) *J. Biol. Chem. 266*, 19543−19550.
63. Kumar, C. C., Nie, H., Rogers, C. P., Malkowski, M., Maxwell, E., Catino, J. J., and Armstrong, L. (1997) *J. Pharmacol. Exp. Ther. 283*, 843−853.
64. Xiong, J. P., Li, R., Essafi, M., Stehle, T., and Arnaout, M. A. (2000) *J. Biol. Chem. 275*, 38762−38767.
65. Emsley, J., Knight, C. G., Farndale, R. W., Barnes, M. J., and Liddington, R. C. (2000) *Cell 100*, 47−56.
66. Shimaoka, M., Shifman, J. M., Jing, H., Takagi, J., Mayo, S. L., and Springer, T. A. (2000) *Nat. Struct. Biol. 7*, 674−678.
67. Cierniewski, C. S., Byzova, T., Papierak, M., Haas, T. A., Niewiarowska, J., Zhang, L., Cieslal, M., and Plow, E. F. (1999) *J. Biol. Chem. 274*, 16923−16932.
68. Hantgan, R. R., Paumi, C., Rocco, M., and Weisel, J. W. (1999) *Biochemistry 38*, 14461−14474.
69. Huang, C., Zang, Q., Takagi, J., and Springer, T. A. (2000) *J. Biol. Chem. 275*, 21514−21524.

BI0109156